Separation mechanisms underlying vector chromatography in microlithographic arrays

Kevin D. Dorfman and Howard Brenner*
Department of Chemical Engineering, Massachusetts Institute of Technology, Cambridge, Massachusetts 02139
(Received 31 July 2001; published 15 May 2002)

Micropatterned chips possessing an asymmetric, spatially periodic array of obstacles enable the vector (directional) chromatographic separation of charged particles animated by an external electric field. We apply a network theory to analyze the chip-scale (L-scale) transport of finite-size Brownian particles in such devices and identify those factors that break the symmetry of the chip-scale particle mobility tensor, most importantly the hydrodynamic wall effects between the particles and the obstacle surfaces. Our analysis contrasts with prevailing separation theories, which are limited to effectively point-size particles, for which wall effects are negligible. These theories require a biasing of obstacle-scale (l-scale; $l \ll L$) bifurcation branches within the network. Such bifurcations are shown to constitute but one factor in modeling the vector chromatography of finite-size particles, and not necessarily the dominant factor.

DOI: 10.1103/PhysRevE.65.052103 PACS number(s): 05.40.Jc, 82.80.Bg, 07.10.Cm, 87.10.+e

The use of microfabricated arrays for the chromatographic separation of Brownian particles, such as biomolecules, proffers great promise as a practical laboratory technique [1]. Such devices typically consist of a spatially periodic, two-dimensional pattern of asymmetrically arranged obstacles embossed on a chip. Particle separation occurs within the solvent-filled channels and their intersections. For charged particles, the separation is effected by applying a time-independent electric field oriented at an angle relative to the lattice axes defining the periodic array [2–4]. On average, different sized particles pursue chip-scale (L-scale) linear trajectories at different angles relative to the pattern. Simultaneously introducing such particles at the same point results in their exit at distinctly different locations along the chip's periphery. In this paper, we demonstrate that this separation arises primarily from the interplay between the particle's Brownian motion and hydrodynamic wall effects [5] connected with the finite size of the particles relative to the interstitial (l-scale) spacing between adjacent obstacles.

In an earlier contribution [6] we classified this type of separation scheme as ''vector'' chromatography to highlight the crucial importance of the mean L-scale *direction* of the particle trajectory. Conventional ''scalar'' (or ''unidirectional'') chromatography, in contrast, relies solely upon the different L-scale mean particle *speeds* achieved through the sorting device. In the latter case, all particles move on average in the same direction, parallel to the animating force.

Our analysis focuses upon solute transport in the long-time limit $t \gg l^2/|\mathbf{D}|$, with l a characteristic linear dimension of the repetitive unit cell and $|\mathbf{D}|$ a suitable norm of the particle's l-scale molecular diffusivity tensor [6]. In chips containing many obstacles [4], this asymptotic limit is easily achieved relative to the nominal holdup time, $t = L/|\overline{\mathbf{U}}^*|$, of the particle as it traverses the entire chip, with L a characteristic linear chip size and $|\overline{\mathbf{U}}^*|$ the chip-scale particle speed.

The proportionality between the applied force $\mathbf{F}$ and a given particle's mean chip-scale vector velocity $\overline{\mathbf{U}}^*$ is expressed by the relation [6]

$$\overline{\mathbf{U}}^* = \overline{\mathbf{M}}^* \cdot \mathbf{F}. \tag{1}$$

The proportionality coefficient $\overline{\mathbf{M}}^*$ is the chromatographic mobility dyadic of that particle, a position- and time-independent constant tensor. For a spherical particle of radius a [$a/l = O(1)$], $\overline{\mathbf{M}}^*$ is a composite phenomenological property of the particle and the chip, being functionally dependent on: (i) the particle radius; (ii) the solvent viscosity; (iii) the chip's lattice axes; (iv) the configuration and orientation of the unit cell (relative to the lattice axes); and (v) the magnitude and orientation of the force $\mathbf{F}$ relative to the lattice. Additional factors would arise for more complex, nonspherical and/or deformable molecules, such as the spring law in a bead-spring polymer model in the latter case [7].

A directional separation is achieved when $\overline{\mathbf{U}}^*$ is not colinear with $\mathbf{F}$, i.e., when $\overline{\mathbf{M}}^*$ is anisotropic. To separate different types of particles, this anisotropy must arise from size- (or charge-) dependent interactions between the Brownian particle and the obstacle surfaces. The extent of vector separation is quantified by the relative discrimination angles, $(\theta_{UF})_i \overset{\text{def.}}{=} \cos^{-1}(\hat{\overline{\mathbf{U}}}_i^* \cdot \hat{\mathbf{F}})$, of different species i ($i = 1,2,\ldots,N$). Here, the caret denotes a unit vector, e.g., $\overline{\mathbf{U}}_i^* = \hat{\overline{\mathbf{U}}}_i^* |\overline{\mathbf{U}}_i^*|$. In contrast, scalar chromatography is quantified by the different *magnitudes*, $|\overline{\mathbf{U}}_i^*|$, of the respective species velocities.

Current theories [2,3] for vector separations are restricted to point-size particles. They postulate a separation mechanism based solely on the following conception: The particle trajectory through a unit cell possesses a bifurcation point, which is caused by the asymmetry of the cell geometry and the particle's molecular diffusivity. The separation is then quantitatively rationalized by a particle-specific probability distribution function (PDF) for particle i ''choosing'' a particular directional bifurcation branch upon exiting a cell and entering the next cell. The PDF is different for different sized particles as a consequence of their different molecular diffusivities. Initial announcements [2] of this separation phenomenon used the name ''rectified Brownian motion'' to

*Email address: hbrenner@mit.edu.

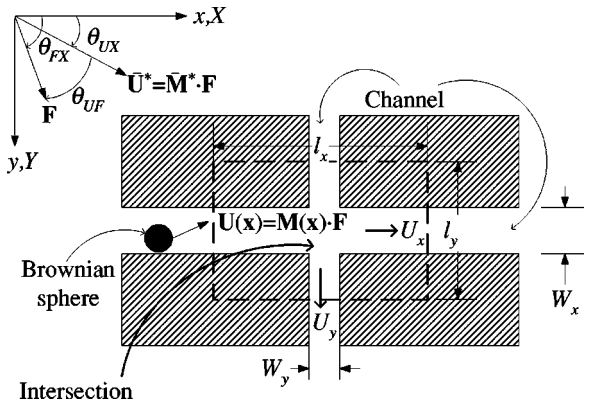

FIG. 1. Spatially periodic microscale rectangular lattice ($l_x \neq l_y$) of rectangular obstacles (shown shaded) spaced at interstitial channel widths $W_x \neq W_y$. The position-independent external force **F** is oriented at an angle θ_{FX} with respect to the x-lattice vector of the array. With its center situated at a point $\mathbf{x} \equiv (x,y)$ within a channel, the sphere moves instantaneously with velocity $\mathbf{U(x)} = \mathbf{M(x)} \cdot \mathbf{F}$. The mean l-scale Taylor-Aris particle velocity components through a channel within a single cell are denoted, respectively, by U_x and U_y. On the chip scale the particle moves, on average, across the chip with its (L-scale) velocity vector $\overline{\mathbf{U}}^* = \overline{\mathbf{M}}^* \cdot \mathbf{F}$. This vector is oriented at an angle θ_{UX} relative to the $x \equiv X$ axis. The disparity in angular direction between $\overline{\mathbf{U}}^*$ and **F** gives rise to the chip-scale discrimination angle θ_{UF}. Notationally, $\mathbf{x} = (x,y)$ are l-scale coordinates ($0 < x < l_x$, $0 < y < l_y$), whereas (X,Y) are L-scale coordinates.

highlight the dependence of the PDF upon such diffusive effects. However, the assumption of point-size particles is contrary to the experiments [4] originally demonstrating such vector separations. In fact, the particles occupied a significant fraction of the interstitial space between adjacent obstacles.

To properly account for hydrodynamic effects, consider the l-scale, interstitial mobility dyadic **M(x)** of a finite-size particle, where **x** refers to the center of the particle. This mobility is both anisotropic and strongly dependent on the instantaneous particle position **x** due to wall effects [5]—even for spherical particles. In what follows, we will show that such wall-induced effects upon the particle's mobility play a crucial role in determining $\overline{\mathbf{M}}^*$ and θ_{UF}, even to the extent of permitting vector separations when the choice of bifurcation branch is totally random.

By way of illustration, as in Fig. 1, consider rectangular obstacles arranged symmetrically in a rectangular array. Here, the lattice axes, characterized by unit vectors $\hat{\mathbf{X}}$ and $\hat{\mathbf{Y}}$, coincide with the obstacle axes (x,y). The charged particle moves through the array under the influence of an external force **F**, which is oriented at an angle θ_{FX} relative to the X axis. Whereas the present analysis explicitly considers spherical particles and rectangular arrays, our eventual conclusions transcend these restrictions. In particular, the spherical particle assumption may be relaxed by employing a mobility dyadic **M(x)** valid for more complex molecules [7].

In general, the chromatographic mobility of a solute particle in a fluid of viscosity η may be expressed as $\overline{\mathbf{M}}^*/6\pi\eta a = \hat{\mathbf{X}}\hat{\mathbf{X}}\overline{M}_X^* + \hat{\mathbf{Y}}\hat{\mathbf{Y}}\overline{M}_Y^*$. (The Stokes law scaling is arbitrary.) Here, for a given particle, the (dimensionless) scalar components $\overline{M}_X^*$ and $\overline{M}_Y^*$ depend functionally on the dimensionless groups characterizing the transport process—explicitly, $\overline{M}_j^* = \overline{M}_j^*(a/W_j, F_j l_j/kT, W_j U_j/|\mathbf{D}|$, etc.), with U_j $[j=(x,y)]$ the Taylor-Aris l-scale average particle speed through a j-directed channel [8]. Vector separation ensues whenever the distinctive particle properties appearing in the arguments of these two mobility components result in the inequality $\overline{M}_X^* \neq \overline{M}_Y^*$ for a given particle i.

To compute $\overline{\mathbf{M}}^*$, we employ a network theory for generalized Taylor-Aris dispersion phenomena, whose details are reported elsewhere [9]. The micropatterned device is represented as a spatially periodic, interconnected network of channels together with their intersections. Classical Taylor-Aris particle velocities and dispersivities [10] are used to quantify the convective-diffusive transport processes occurring in these channels. When the particle is present within an intersection, the choice of the particle's intersection egress channel is assumed to be furnished by a particle-size-dependent ''mixing rule,'' which simulates the physical transport processes occurring within that intersection. In contrast with prior models [2,3], this fact is not essential to the vector separation phenomenon because of our incorporation of hydrodynamic wall effects. We will focus only on the task of establishing the *direction* of the particle trajectory, although the general theory [9] permits a complete Taylor-Aris dispersion analysis, including calculation of the chip-scale particle velocity $\overline{\mathbf{U}}^*$.

The network depicted in Fig. 1 is a so-called ''simple network'' [9], consisting of a single intersection joining together x- and y-directed channels at their openings. The particle's probability density is trivial—the particle must be located within the single nodal area contained within the unit cell boundaries. Consequently, computing $\overline{\mathbf{U}}^*$ simply necessitates defining: (i) the particle's probability density ''flow rate'' Q_j within x- and y-directed channels; and (ii) the probability ratio K of the particle choosing x- and y-directed channels at the intersections.

For a given particle, the probability flow rate through channel j is given by $Q_j = \mu_j F_j W_j$, with μ_j the particle's l-scale mean mobility in channel j, F_j the component of the external force along the direction of the channel, and W_j the channel width. When $l_j \gg W_j$, μ_j possesses its classical Taylor-Aris dispersion value in the channel [10], which includes a Boltzmann bias arising from the action of the transverse force:

$$\mu_j = \frac{\int_0^{W_j} dx_k M_{jj}(x_k) \exp(F_k x_k/kT)}{\int_0^{W_j} dx_k \exp(F_k x_k/kT)} \quad (j,k=x,y; j \neq k), \tag{2}$$

where M_{jj} is the component of **M(x)** in the j direction and kT is the Boltzmann factor. For spherical particles and planar channel geometries, the pointwise mobility dyadic **M(x)**, in-

cluding wall effects, is available from rigorous hydrodynamic theory [11,12]. For more complex molecules, it remains possible to make this calculation using an approximate hydrodynamic theory [13]. When the chip geometry and/or the molecular shape exceed computational resources, μ_j may be determined from experiments performed using a single channel of large aspect ratio, $l_j \gg W_j$. Equation (2) is a generic result, rendering later conclusions based upon μ_j [cf. Eq. (3)] independent of our spherical particle assumption.

Quantifying K depends upon the particle Peclet number, Pe, representing the ratio of convective to diffusive transport rates within the intersection. Perfect mixing [14] is assumed for diffusion-dominated transport, $\mathrm{Pe} \ll 1$, so that all intersectional egress channels are equally probable. This corresponds to randomizing the choice of bifurcation branch in existing point-size theories [2,3]. For convection-dominated transport, $\mathrm{Pe} \gg 1$, the choice of intersectional egress channel is assumed to be proportional to the channel's flow rate Q_j [15]. Any value of Pe can be encompassed by defining the partition coefficient, $K = \mathrm{Prob}(y)/\mathrm{Prob}(x)$, with $\mathrm{Prob}(j)$ the probability of the particle entering channel j upon exiting the intersection. Consequently, $K=1$ and $K = Q_y/Q_x$ in the respective low and high Péclet number limits.

The preceding analysis, when brought to fruition [9], enables the particle's chip-scale velocity components $\overline{U}_X^*$ and $\overline{U}_Y^*$ to be explicitly calculated. The angle θ_{UX} formed by $\overline{\mathbf{U}}^*$ and the X axis is given by

$$\tan \theta_{UX} \overset{\text{def.}}{=} \frac{\overline{U}_Y^*}{\overline{U}_X^*} = \mu K \frac{W_y l_y}{W_x l_x} \frac{F_y}{F_x}, \tag{3}$$

with $\mu \equiv \mu_y/\mu_x$. The discrimination angle is then computed by

$$\theta_{UF} = \theta_{UX} - \tan^{-1}(F_y/F_x). \tag{4}$$

This analysis also furnishes the components $\overline{M}_X^*$ and $\overline{M}_Y^*$ of $\overline{\mathbf{M}}^*$, since $\overline{U}_X^*$ and $\overline{U}_Y^*$ are related to F_x and F_y by Eq. (3).

Several generic geometric conclusions are apparent from Eq. (4). First, when **F** is applied along a symmetry axis of the array (the X or Y direction), the discrimination angle $\theta_{UF} = 0$ and is independent of the particle properties. Second, for point-sized particles and perfect mixing ($\mu = K = 1$), θ_{UF} is characterized exclusively by the symmetry group of the ''composite'' $l \oplus L$-scale array geometry. Explicitly, the spatial arrangement of the obstacles determines the L-scale lattice symmetry, whereas the obstacle's shape determines the l-scale point-group symmetry class. The symmetry of the composite $l \oplus L$ array consists of common symmetry elements, if any, between the respective lattice and obstacle point-group rotational symmetries. These symmetries need not be the same; for example, regular pentagon-shaped objects in a rectangular array possess no common symmetry elements (except for a center of symmetry), irrespective of the orientation of the obstacles relative to the lattice.

To clarify the preceding comments, we examine the array depicted in Fig. 1. When $W_x = W_y$ and $l_x = l_y$, the array consists of square obstacles in a square lattice, with coincident rotational symmetry axes. The fourfold $l \oplus L$ composite symmetry [16] of this array makes $\overline{\mathbf{M}}^*$ isotropic and $\theta_{UF} = 0$, irrespective of the orientation of **F** relative to the lattice axes. In contrast, an array with $W_x \neq W_y$ or $l_x \neq l_y$ represents either square objects in a rectangular array or rectangular objects in a square array. These lattices only possess twofold rotational symmetry. Second-rank tensors associated with twofold symmetry are anisotropic [17], so particle motion is no longer colinear with the force. However, vector separation requires that the physical attributes of the particles cause the anisotropy. If the anisotropy is attributable only to the array symmetry, then all particles will move on average in the same direction, albeit in a direction no longer colinear with the force.

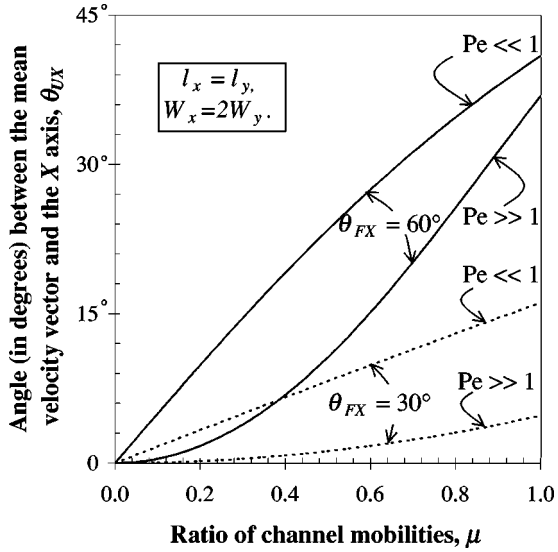

FIG. 2. Angle θ_{UX} formed between the particle's chip-scale mean velocity vector $\overline{\mathbf{U}}^*$ and the X axis for the conditions indicated in the inset. Solid and dashed lines correspond to angles $\theta_{FX} = 60°$ and 30°, respectively, between the applied force **F** and the X axis.

Thus, vector separation is possible only when the parameters μ and K appearing in Eq. (3) differ between particles. Existing theories [2,3] consider the case where K (but not μ) is a function of the particle properties. When wall effects are substantial, the simplest method for altering μ is to construct an array with different gap widths, namely $W_x \neq W_y$. Variable gap widths have a nonlinear effect upon the channel particle mobilities μ_j via (2), as well as imparting twofold symmetry to the array. Alternatively, even for fourfold symmetric arrays, the presence of a strong transverse force, $F_j \gg F_k$, in one of the channels biases μ_j as a consequence of the Boltzmann factor in (2). In either case, the chromatographic mobility $\overline{\mathbf{M}}^*$ no longer possesses the fourfold point-group symmetry characterizing the array geometry. This symmetry-breaking feature underlies the fundamental mechanism of vector chromatography.

Consider the explicit example of a square lattice $l_x = l_y$ with rectangular obstacles separated by distances $W_x = 2W_y$. The relative widths impart a wall-effect-induced

preference for particle motion in x direction, as well as imposing the inequality $\mu \leqslant 1$. Figure 2 depicts the angle θ_{UX} as a function of μ, for the limiting cases of both perfect mixing and convection-dominated transport at the intersection. For point-size particles ($\mu = 1$), we see that the twofold symmetry of the array results in $\theta_{UX} \neq \theta_{FX}$. For finite-size particles, vector chromatography is possible even for the case where $K = 1$, where the bifurcation branch is totally random. The range of available angles θ_{UX} is small when applying the force at the angle $\theta_{FX} = 30°$. This makes a vector separation difficult. In contrast, applying the force at an angle $\theta_{FX} = 60°$—"against" the preferred direction—makes for an easier vector separation. This increased efficiency accords with experimental results [4], where the greater component of the force coincided with the narrower channel.

We are grateful to Dr. Sangtae Kim of Eli Lilly and Company for his interest and encouragement in our microfluidic analyses and to Professor Howard A. Stone of Harvard for useful discussions.

[1] T. Duke, G. Monnelly, R. H. Austin, and E. C. Cox, Electrophoresis **18**, 17 (1997).
[2] T. A. J. Duke and R. H. Austin, Phys. Rev. Lett. **80**, 1552 (1998).
[3] D. Ertas, Phys. Rev. Lett. **80**, 1548 (1998).
[4] C. F. Chou *et al.*, Proc. Natl. Acad. Sci. U.S.A. **96**, 13 762 (1999); C. F. Chou *et al.*, Electrophoresis **21**, 81 (2000).
[5] H. Brenner and L. J. Gaydos, J. Colloid Interface Sci. **58**, 312 (1977).
[6] K. D. Dorman and H. Brenner, J. Colloid Interface Sci. **238**, 390 (2001).
[7] R. B. Bird, C. F. Curtiss, R. C. Armstrong, and O. Hassager, *Dynamics of Polymeric Liquids* (Wiley, New York, 1987), Vol. II.
[8] Majuscule indices refer to L-scale directions (X,Y) and miniscule indices to l-scale directions (x,y).
[9] K. D. Dorfman and H. Brenner, Phys. Rev. E **65**, 021103 (2002).
[10] H. Brenner and D. A. Edwards, *Macrotransport Processes* (Butterworth-Heinemann, Boston, 1993).
[11] J. Happel and H. Brenner, *Low Reynolds Number Hydrodynamics* (Kluwer, Netherlands, 1983).
[12] S. Kim and S. J. Karrila, *Microhydrodynamics* (Butterworth-Heinemann, Boston, 1991).
[13] R. M. Jendrejack, M. D. Graham, and J. J. DePablo, J. Chem. Phys. **113**, 2894 (2000).
[14] P. M. Adler and H. Brenner, PCH, PhysicoChem. Hydrodyn. **5**, 269 (1984).
[15] M. Sahimi, H. T. Davis, and L. E. Scriven, Chem. Eng. Commun. **23**, 329 (1983).
[16] Were the point-group symmetry rotation axes of the square obstacles not aligned with those of the square lattice, the only common symmetry element would be a center of symmetry. Consequently, the array would no longer be isotropic with respect to second-rank tensors.
[17] A. R. Billings, *Tensor Properties of Materials* (Wiley, New York, 1969).